Longe Range Particle Collisions for the PIC/DSMC Simulation Code PicLas

IEPC-2007-36

Presented at the 30th International Electric Propulsion Conference, Florence Italy, September 17 – 20, 2007

Danilo D'Andrea[a] and Rudolf Schneider[b]

Forschungszentrum Karlsruhe - in der Helmholtz-Gemeinschaft, Institut für Hochleistungsimpuls und Mikrowellentechnik, D-76021 Karlsruhe, Germany
Partner of Karlsruhe Institute of Technology

Martin Quandt[c] and Claus-Dieter Munz[d]

Institut für Aerodynamik und Gasdynamik, Universität Stuttgart, D-70550 Stuttgart, Germany

Sabine Roller[e]

Höchstleistungsrechenzentrum Stuttgart, D-70550 Stuttgart, Germany

Markus Fertig[f]

Institut für Raumfahrtsysteme, Universität Stuttgart, D-70550 Stuttgart, Germany

The modeling and simulation of highly rarefied plasma flows is an important item to get a deeper physical understanding of electric propulsion systems like pulsed plasma thrusters. For that purpose the PIC/DSMC (Particle in Cell / Direct Simulation Monte Carlo) simulation code PicLas is under development at Stuttgart University and Research Center Karlsruhe. A central building block of the PicLas Code is the Fokker-Planck solver on which we will focus our attention in the following. This solver allows the treatment of long range inter- and intra-species particle interaction. The numerical modeling of charged particle collisions in a plasma will be explained in some detail and results will be presented.

[a]Scientist, danilo.dandrea@ihm.fzk.de
[b]Senior Fellow, rudolf.schneider@ihm.fzk.de
[c]Scientist, quandt@iag.uni-stuttgart.de
[d]Professor, munz@iag.uni-stuttgart.de
[e]Scientist, Department for Applications, Models and Tools, roller@hlrs.de
[f]Head of Plasma Modelling and Simulation Group, Raumtransporttechnologie, fertig@irs.uni-stuttgart.de

Nomenclature

$\vec{c}$, $\vec{w}$	particle velocity
f	velocity distribution function
$\vec{g}$	relative velocity vector
g	relative velocity
n	particle density
t	time
$\vec{x}$	spatial coordinates vector
$\mathbf{D}$	diffusion tensor
$\vec{F}$	friction force vector
H	Boltzmann's H-function
$\mathcal{H}, \mathcal{G}$	Rosenbluth potentials
$\mathbf{B}$	associated diffusion tensor
Δt	time step size
$d\vec{W}$, $\Delta\vec{W}$	Wiener increment

Greek Symbols

μ	mean value
σ^2	variance
σ_{ij}	collision cross section
τ	time constant
Ω	solid angle

Constants

Γ_P	plasma parameter

Subscripts

col	Collisions
e	electron
i, j	species indices

Abbreviations

BG	**b**ack**g**round
DSMC	**D**irect **S**imulation **M**onte **C**arlo
FFT	**F**ast **F**ourier **T**ransformation
FP	**F**okker **P**lanck
HLRS	**H**öchst**l**eistungs**r**echenzentrum **S**tuttgart
IAG	**I**nstitut für **A**erodynamik und **G**asdynamik
IHM	**I**nstitut für **H**ochleistungsimpuls und **M**ikrowellentechnik
IRS	**I**nstitut für **R**aumfahrt**s**ysteme
PIC	**P**article **i**n **C**ell
PPT	**P**ulsed **P**lasma **T**hruster
SDE	**S**tochastical **D**ifferential **E**quation

I. Introduction

In order to model electric propulsion systems like PPT, a cooperation between several institutes of Stuttgart University (IRS, IAG and HLRS) and Research Center Karlsruhe (IHM) has been formed to develop the hybrid PIC/DSMC code named PicLas[1,2] This code solves the Boltzmann equation for different physical regimes, to simulate the rarefied, non-continuum plasma flow in the thrusters. To include the relevant physics, the PIC scheme developed by IHM[3,4] is being extended by adding models for intra- and inter- species charged particle collisions and intermolecular reactions (see Figure 1). The block diagram in Figure 1 illustrates schematically the working principles of the new code. The Maxwell-Vlasov solver models the interactions between charged particles and electromagnetic fields. Momentum and energy exchanges, without consideration of Lorentz force, as well as chemical reactions are treated in DSMC block, by means of a DSMC method based on the previous "LasVegas" code.[5] Finally, the effects of electrons and ions collisions on their velocity field are evaluated in the completely new Fokker-Planck solver, which adopts PIC techniques in velocity space. The integration of these three models is expected to allow for an accurate prediction of the behaviour of electric space propulsion systems operating far from continuum hypotheses. Additionally, the necessity of a three dimensional and time accurate description and complex geometries requires optimization and parallelization of the code in order to efficiently use high performance computers.
The general program structure of the coupled code PicLas allows for a flexible combination of the different modules which will be run in parallel mode, each to contribute to the final $\Delta\vec{V}$.

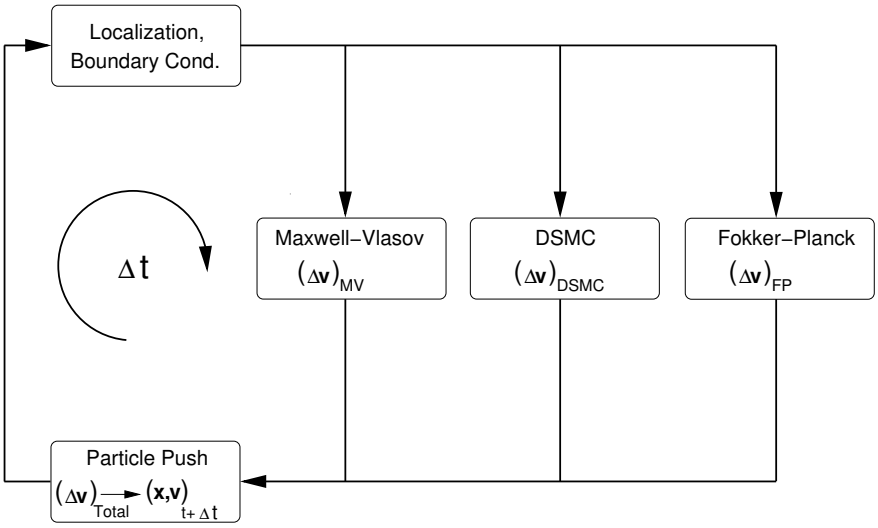

Figure 1. Schematic view of the coupling concept

The interplay of the different building blocks will be investigated and analyzed in detail. Due to the multi-scale nature of the problem, the requirements for time step size, mesh size w.r.t. mean free path length, the maximum or minimum number of particles per cell might be competing, and systemic rules for stable, accurate settings are under development.
In the present paper, we focus our attention to the Fokker-Planck building bock where the electron-electron collisions – abbreviated by (e,e) – and electron-ion collisions – abbreviated by (e,I) – in the plasma under consideration are treated. We assume that the electron density is of the order of $10^{18}\,\mathrm{m}^{-3}$, which means that the (e,e)-collision frequency exceeds the one of electron-neutral collisons. It is obvious that in such plasmas the shape of the electron energy distribution function (EEDF) is mainly determined by the (e,e)-interactions. In the case where the energy input into the plasma goes primarily into the thermal part of the EEDF, the high-energy tail is mainly populated by energy up-scattered electrons caused by (e,e)-collisions, which always drive the EEDF towards a Maxwellian distribution. Deviation from such ideal behaviour are caused for example, by inelastic electron-neutral collisions which deplete the high energy tail, and in bounded

plasmas whose walls the fastest electrons can escape through. Furthermore, energetic considerations indicate that the high-energy tail controls reactions like atomic excitation and ionization, and to some extent the plasma chemistry. Clearly, since the EEDF determines many properties of the plasma, it is essential to model (e,e)-collisions as realistic as possible. In the following, we describe the formulation that allows to include (e,e)-collisions into a PIC framework in a natural way. Therefore, in Section II the governing equations and the numerical framework are introduced. Results obtained from several numerical experiments are presented in Section III and finally, a short summary and an outlook of our further activities are given in Section IV.

II. Mathematical and Numerical Modelling of Coulomb Interaction

In order to describe the non-continuum plasma flow in the thruster, a general starting point is the Boltzmann equation, which describes the change of the velocity distribution f_i for the specie "i" in time and phase space as a result of external forces and particle collisions. To determine the transient, local velocity distribution function, the different contributions to the Boltzmann equation are decoupled and treated separately according to the physical situation on hand. In this context we are concerned with the rate of change of f_i over time due only to collisions. The Boltzmann collision integral[6] reads as

$$\left(\frac{\delta f_i}{\delta t}\right)_{Col} = \sum_j n_j \int g(\vec{c}_i, \vec{c}_j)\, \sigma_{ij}(g, \vec{g}\cdot\vec{g}')\Big[f_i'(\vec{c}'_i)\, f_j'(\vec{c}'_j) - f_i(\vec{c}_i)\, f_j(\vec{c}_j)\Big]\, d\Omega\, d\vec{c}_j \ . \tag{1}$$

Here, the index j stands for all "scattering" populations, $n_j = n_j(\vec{x}, t)$ is the density of species "j", $\vec{g} = \vec{c}_i - \vec{c}_j$ represents the difference between the velocity $\vec{c}$ of the scattered-off electrons and the velocity of the electrons that serve as scatterers, $\sigma_{ij}(g, \vec{g}\cdot\vec{g}')$ is the differential scattering cross section between the particles of the species "i" and "j", and the differential solid angle $d\Omega$ is given by $d\Omega = \sin\theta\, d\theta\, d\phi$. The primed quantities refer to the value after a collision and the unprimed ones denote the pre–collisional values.
In order to consider exclusively elastic intra-species long range electron-electron and ion-ion collisions as well as elastic inter-species electron-ion Coulomb scattering it is sufficient to use the Fokker-Planck equation to approximate the collision integral (1). Clearly, in this case $\sigma_{ij}(g, \theta)$ is given by the classical Rutherford differential cross section (see, for instance Ref.[7]), where θ is the scattering angle.

A. The Fokker-Planck Equation

For sake of clarity, we restrict the following analysis to the case of intra-species collisions only, in particular (e-e), since the electron-ion interactions can be derived straightforeward.[8] The Fokker-Planck equation

$$\left(\frac{\delta f_e}{\delta t}\right)_{Col} = -\nabla_c\Big[\vec{F}\, f_e\Big] + \frac{1}{2}\nabla_c^T\Big[\nabla_c^T\left(\mathbf{D}\, f_e\right)\Big]^T \ , \tag{2}$$

with $\nabla_c = \left(\partial/\partial c_1, \partial/\partial c_2, \partial/\partial c_3\right)^T$ describes the evolution of the electron distribution function $f_e = f_e(\vec{x}, \vec{c}, t)$ as a result of small-angle scattering of Coulomb point particles, and represents the lowest order approximation of the Boltzmann collision integral.[9, 10, 11] The components of the friction force (or drift) vector $\vec{F}$ and the diffusion tensor $\mathbf{D} \in \mathcal{R}^{3\times 3}$ are given by

$$F_\alpha(\vec{x}, \vec{c}, t) = \Gamma_P\, n_e(\vec{x}, t)\, \frac{\partial \mathcal{H}}{\partial c_\alpha} \ , \quad \alpha = 1, 2, 3 \tag{3}$$

and

$$D_{\alpha\beta}(\vec{x}, \vec{c}, t) = \Gamma_P\, n_e(\vec{x}, t)\, \frac{\partial^2 \mathcal{G}}{\partial c_\alpha \partial c_\beta} \ , \quad \alpha, \beta = 1, 2, 3 \ , \tag{4}$$

respectively, where $n_e(\vec{x}, t)$ is the local electron density and $\Gamma_P = \frac{e^4}{4\pi\epsilon_0^2 m_e^2}\ln(\Lambda)$ denotes the plasma parameter with the Coulomb logarithm $\ln(\Lambda)$ (see, e.g. Ref.[6]). The key quantities to compute these coefficients

are the Rosenbluth potentials[7] which are defined according to

$$\mathcal{H}(\vec{x},\vec{c},t) = 2\int\limits_{-\infty}^{\infty} d^3w\ |g|^{-1}\, f_e(\vec{x},\vec{w},t) \quad \text{and} \quad \mathcal{G}(\vec{x},\vec{c},t) = \int\limits_{-\infty}^{\infty} d^3w\ |g|\ f_e(\vec{x},\vec{w},t)\ . \tag{5}$$

Clearly, the friction force $\vec{F}$ and the diffusion tensor $\mathbf{D}$ themselves depend on the velocity $\vec{c}$ and, hence, the FP model generally is a complicated non-linear problem that has to be solved numerically in an appropriate – namely, self-consistent – manner. The direct numerical solution of the FP equation can now be performed, and at the end of this paragraph we will make clear the link between such a procedure and the desired PIC method.[12] It is well known that the assumption of an isotropic but non-Maxwellian velocity distribution of the scatterer implies an enormous reduction of the problem since the diffusion and friction coefficients can be written in terms of one-dimensional quadratures.[7,12,13] However, in cases where no model assumptions concerning the distribution function can be imposed, a 3D quadrature formula would be very time consuming. A deeper observation of (5) reveals that the Rosenbluth potentials are convolutions of the scatter distribution functions and of the absolute value of the relative speed. This suggest to apply Fourier transformation techniques to compute the integrals, where no model assumptions concerning the distribution function have to be imposed. After some standard manipulations,[14] we obtain the results

$$\mathcal{H}(\vec{c}) = 8\,\pi\mathcal{F}^{-1}\left\{\frac{\hat{f}_e(\vec{k})}{k^2}\right\} \tag{6}$$

and

$$\mathcal{G}(\vec{c}) = -8\,\pi\mathcal{F}^{-1}\left\{\frac{\hat{f}_e(\vec{k})}{k^4}\right\}\ , \tag{7}$$

where the identity $\nabla_{\vec{c}}^2 g = 2/g$ has been used to obtain the second relation and $\mathcal{F}^{-1}$ denotes the inverse Fourier transformation of the arguments in the braces. Clearly, the argument of (6) reveals the convolution character of first expression in (5), which means that we get in $\vec{k}$-space the product of the Fourier transform $\hat{f}_e(\vec{k}) = (2\pi)^{-3/2}\int\limits_{-\infty}^{\infty} d^3c\,\mathrm{e}^{-i\,\vec{k}\cdot\vec{c}}\, f_e(\vec{c})$ and $1/k^2$, which is the Fourier transformation of the "Coulomb potential" $1/g$. Since the derivatives of the Rosenbluth potentials enter into the determinations (3) and (4), we apply the differentiation property of the Fourier transformation and find immediately

$$\frac{\partial\mathcal{H}}{\partial c_\alpha} = 8\,\pi\,i\mathcal{F}^{-1}\left\{\frac{k_\alpha}{k^2}\,\hat{f}_e(\vec{k})\right\} \quad \text{and} \quad \frac{\partial^2\mathcal{G}}{\partial c_\alpha\partial c_\beta} = 8\,\pi\mathcal{F}^{-1}\left\{\frac{k_\alpha k_\beta}{k^4}\,\hat{f}_e(\vec{k})\right\}\ . \tag{8}$$

Note, that such a determination of the derivatives may considerable reduce "computational noise" which is often associated with finite difference differentiation on the velocity grid.

In essence, the main advantage of the Fourier approach is that we obtain a first principle, fully self-consistent determination of the deterministic friction and stochastic diffusion arising in (2) since no specific model assumptions are necessary to compute the Rosenbluth potentials. Consequently, the (e,e)-collisional relaxation is modeled in a complete self-consistent way. Furthermore, note that the appearence of the FP equation reveals that the (e,e)-collisions are modeled as a diffusion process that describes the short-time behavior of the considered system.[15,16]

Making use of the Itô formula[15,17] one can show that the FP equation (2) for the evolution of f_e is equivalent to the stochastical differential equation (SDE) of Langevin-type

$$d\vec{C}(t) = \vec{F}(\vec{C},t)\,dt + \mathbf{B}(\vec{C},t)\,d\vec{W}(t)\ , \tag{9}$$

where $\vec{W}(t) \in \mathcal{R}^3$ represents the three-dimensional Wiener process and the matrix $\mathbf{B} \in \mathcal{R}^{3\times3}$ is related to the diffusion matrix according to $\mathbf{D} = \mathbf{B}\,\mathbf{B}^T$. As indicated, both quantities $\vec{F}$ and $\mathbf{B}$ now depend on the stochastic variable $\vec{C} = \vec{C}(t)$, which will be identified later as the velocity of the (macro) electrons. We remark that the Langevin-type equation takes the role of the deterministic Lorentz equation in the classical PIC approach, but for numerical purposes this equation has to be discretized within the framework of stochastic calculus. Hence, the use of the Langevin-type SDE (9) fits in a remarkable way into the standard PIC approach,[3] which is one basic concept of the PicLas code development.

B. Numerical Framework: The PIC Approach

The numerical solution of the FP equation is illustrated in the block diagram below. The analogy with classical PIC concept is immediately evident: One part of the cycle is situated in a mesh-free zone, while another one needs a discretization grid, with two interfaces procedures closing the whole calculation.

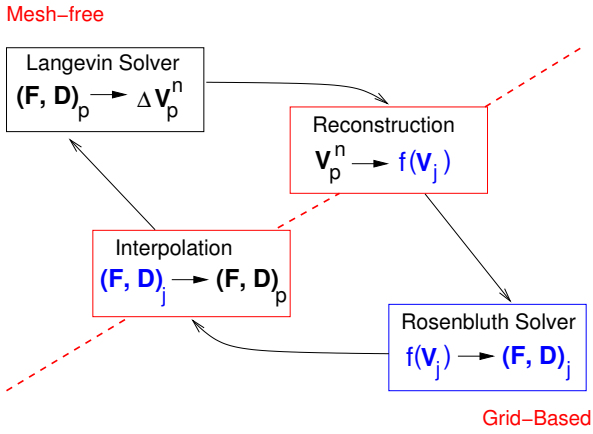

Figure 2. Building blocks of the PIC approach for the Fokker-Planck equation.

In the following, a short description of the single building blocks of the Fokker-Planck solver is given.
Assignment and Reconstruction. From the actual location of the plasma particles in the three-dimensional mesh-free velocity space, the distribution function $f_e(\vec{c})$ is resolved on the Cartesian velocity mesh. For that, we apply the volume-weighting technique[18,8] to compute relative weighting coordinates for each particle "p" from which individual particle weights $g^{(p)}$ can be determined. These particle weights then contain the necessary information to assign each particle to the corresponding grid cell of the velocity mesh.
Rosenbluth Solver. Afterwards, for the grid-based computations a FFT method similar to the Cooley and Tukey algorithm[19,20] is applied to compute the Fourier transform $\hat{f}_e(\vec{k})$ of the distribution function $f_e(\vec{c})$. Subsequent multiplications of $\hat{f}_e(\vec{k})$ with $1/k^2$, k_α/k^2, etc. and a final inverse transformation yields the grid-based Rosenbluth potentials (6) and (7) and, especially, their derivatives with respect to the velocity (8), from which the components of the friction force vector (3) and the diffusion matrix (4) can immediately be determined.
Interpolation. The "Langevin forces", which are the deterministic friction and the stochastic diffusion, have to be computed at the actual position of each particle in grid-free velocity space. Since interpolation is nothing else than the inverse operation of assignment, the particle weights $g^{(p)}$ are once again used to interpolate the Langevin forces at the position of particle "p" in continuous velocity space (see, for instance Ref.[18,8]).
Langevin Solver. Under the action of the velocity-dependent Langevin forces, each particle is moved in velocity space according to the SDE (9), where appropriate numerical methods are required. For our purposes, we use weak approximations[17] of equation (9). Therefore, we perform an Itô-Taylor expansion up to the terms whose multi-indices belong to a desired hierarchical set. For instance, the simplest multi-dimensional weak Taylor expansion leads to the Euler scheme[21]

$$\vec{C}^{n+1} = \vec{C}^n + \vec{F}(\vec{C}^n, t^n)\,\Delta t + \sum_{\alpha=1}^{3} \vec{b}_\alpha(\vec{C}^n, t^n)\,\Delta W_n^\alpha \;, \tag{10}$$

which converges weakly with order $\beta = 1.0$. Here, $\vec{b}_\alpha = \mathbf{B}\cdot\vec{e}_\alpha$, with unit vector $\vec{e}_\alpha$, and the Wiener increment ΔW_n^α is defined according to $\Delta W_n^\alpha = \sqrt{\Delta t}\,\eta_\alpha$, where Δt is the time step size and $\eta_\alpha \sim \mathcal{N}(0,1)$ denotes a Gaussian distributed random number with mean $\mu = 0$ and variance $\sigma^2 = 1$. Note, that in the situation of weak approximation the Gaussian random number ΔW_n^α can be substituted by a simpler random number $\Delta\hat{W}_n^\alpha$ which is two-point distributed.[17]

The convergence order of the Euler scheme can easily be improved by adding the derivatives of various orders of the friction and diffusion coefficients which have to be replaced by appropriate approximations.[17]
This step closes the self-consistent determination cycles, which have to be run through at each time step and for each spatial grid cell.

III. Results

Each single block has been tested in its 3D version separately[8] providing very good reliability. We present here the validation of the whole Fokker-Planck module by means of a sequence of numerical experiments demonstrating the good approximation properties of the introduced schemes. In order to perform a general investigation about intra-species collisions, all the quantities have been treated as dimensionless quantites. As reference sizes we considered the mass and charge of electrons with a number density of 10^{18} m^{-3}. The thermal velocity is derived from a Maxwellian distribution function of electrons at a temperature of 10 eV. From these parameters one obtains that one time unit is equivalent to $1.78 \cdot 10^{-7}$ seconds.

A. Experiment 1: Reservoir Simulation

For sake of clearness, we consider in the following a single spatial grid cell, in which a sufficient large number of particles ($N_p = 3 \cdot 10^5$) is located, and assume that the computational Cartesian mesh in velocity space is associated with this local grid zone. The initial state is prepared assigning to each velocity component a Gaussian velocity distribution all with mean zero but with different variances (temperatures): $\sigma_1^2 = 1.0$, $\sigma_2^2 = 2.25$ and $\sigma_3^2 = 4.0$. Afterwards, the system evolves through intra-species Coulomb scattering up to time $t = 150$, where $\Delta t = 5 \cdot 10^{-2}$. It is well-known that the FP operator acting on f_e (2) is dissipative in the sense of satisfying Boltzmann's H-theorem.[22] In other words a system of charged particles in non-equilibrium condition evolves in the course of time to its equilibrium conditions and relaxes to a Maxwellian shaped distribution with positive entropy production. A figure of merit in this context is the local H-function applied in the form

$$H(\vec{x},t) = -\int\limits_{R^3} d^3c \, [\ln f_e(\vec{c},\vec{x},t)] \; f_e(\vec{c},\vec{x},t) \; , \tag{11}$$

which can be ascribed to Boltzmann. Obviously, $H(\vec{x},t)$ can be regarded as a measure of the extent to which the conditions of a system deviate from that corresponding to equilibrium. It can further be shown[23] that when the equilibrium is reached, collisions are not responsible anymore for the rate of change of $H(\vec{x},t)$. The temporal evolution of the H-function obtained from different numerical experiments are depicted in Figure 3. Clearly, the H-function measured on the velocity grid with 64 nodes per direction (dashed line) shows an increasing behavior with time. This artificial warming (the variance increases also; not shown here), almost linear in time, may be attributed to the "particle sharing" of the nodes and interpolation of the "node values" to the particles.[18] As seen in Figure 3, it is possible to control this phenomenon to some extent by increasing the number of grid points (dashed-dotted line: 128 nodes per direction). Now, the increase of H with time is less pronounced. The remaining increase of H may be led back to the first order approximation of the assignment and interpolation procedure.[18] In order to get completely rid of the numerical errors we adapted the renormalization procedure

$$\vec{v}_\alpha \rightarrow \vec{V}_\alpha = \vec{\mu} + \left(\vec{v}_\alpha - \vec{\mu}^{\,\prime}\right)\sqrt{\frac{(\sigma^2)}{(\sigma^2)^\prime}} \; ; \quad \alpha = 1, \ldots, N_p \tag{12}$$

originally introduced by Lemons et al.[24] to cure instability problems arising in finite samples simulations. Here, $\vec{\mu}$ and (σ^2) are the desired mean and variance while prime symbol indicate the actual values. The renormalization (12) eliminates any instabilizing fluctuations in the moments of f_e by linear transforming the particles velocities without changing the shape of the distributions so that their means and variances recover the desired values while the system evolves stochastically. As shown by the bold line in Figure 3, no unreal heating takes place and once the equilibrium is attained the H-function stays – besides small oscillations –

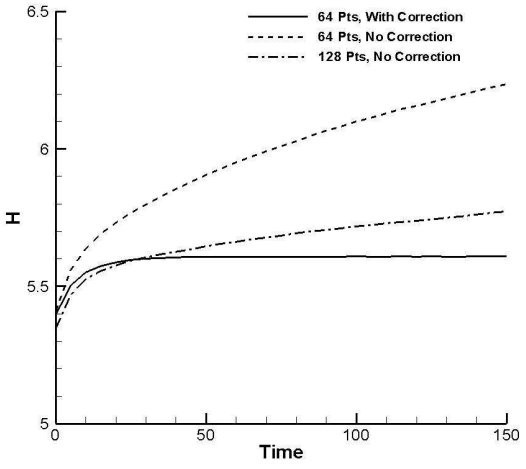

Figure 3. Temporal evolution of Boltzmann's H-function. Dashed line: 64 nodes per dirction, dashed-dotted line: 128 nodes per dirction, full line: 64 nodes per dirction and correction.

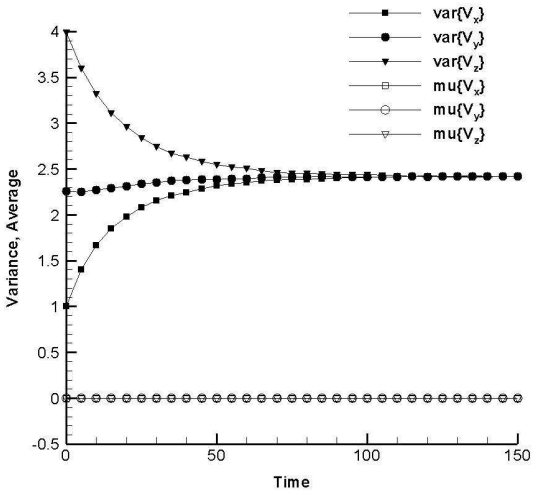

Figure 4. Temporal evolution of the variances σ_1^2 (line with full squares), σ_2^2 (line with full circles) and σ_3^2 (line with full gradients). The lines with open symbols show the mean values of the velocity components which all stay equal to zero.

constant. This correction assures also that mean energy (temperature) and momentum are conserved during the simulation.

Further numerical results which are measured from particle quantities are shown in Figure 4, where the correction (12) is now applied. As observed there, the mean values of all velocity components remain constant (namely zero) since there is no external force to cause a stream motion of the particles. The diffusion process established by the FP (2) (or the Langevin-type (9)) provides, by means of the friction and diffusion forces, mechanisms that allow internal energy exchanges such that the system reaches the thermal equilibrium in agreement with the equipartition principle. As long as the system approaches this state, very small changes take place in the distribution functions form. Even if they are still visible in particle quantities (Figure 4) they can hardly be catched by an integration on grid, resulting in a underestimation of the relaxation time (Figure 3).

B. Experiment 2: Characteristic Time Scales

We are often interested to know the time in which collisions can produce large alteration in the original velocity distribution; for example how rapidly an initial anisotropic distribution function relaxes to a Maxwellian because of collisions. The time required for the whole process to take place is known as "relaxation time" and it is clearly a not defined one.[25] One way to obtain estimations of such parameter is to consider the scattering of one particle and try to get information about the time scaling of a distribution of particles with the same initial velocity conditions. This classical method known as test-particle approach was developed by Chandrasekhar[26] and Spitzer,[25] and a variation can be found, for instance, in Montgomery & Tidman.[10] One relaxation time investigated by the test-particle method is the so-called slowing down time. This time scale gives rate at which collisions decrease the mean velocity of the test particles. These particles are initially "injected" into the plasma as a monochromatic "beam" which has only a constant c_z velocity component and are "traced" up to the time where they are stopped. Note that it can be shown[10] that the slowing down time is only related to the friction force coefficients of the FP equation. Another relaxation time of interest in the test-particle approach is the so-called deflection time, which may be considered as the typical time scale for an initially anisotropic distribution becomes isotropic.[6] Per construction this time scale is associated with the transverse velocity components of the test particles which are zero initially and is a measure of

gradual deflection of the test particles by 90 degrees caused by the cumulative effects of collisions. Simple considerations reveal that the rate of increase of the transversal velocities is only due to the diffusion term of the FP equation.[10] For the parameters used below one obtains for the slowing down and deflection time the values $\tau_{slo} \approx 62.25$ and $\tau_{def} \approx 130.3$, respectively.
In the context of the present paper we intend to study the self-consistent dynamical evolution of the velocity distribution, where both friction force and diffusion are similarly important. Clearly, to switch off one of the dynamical aspects seems to be idle but would contradict our self-consistent approach. In order to filter out characteristic times required by a whatever distribution function to reach an equilibrium state because of collisions we propose the following proceeding. The particles in the numerical experiments are subdivided in two groups: The first one consists of the background (abbreviated by BG) particles (constant number $N_{BG} = 3 \cdot 10^5$) which are Maxwellian distributed (that is Gaussian distributed in each velocity component; $\mu_{BG} = 0.$, $\sigma^2_{BG} = 1.$) initially, and the second group is the beam particles (labelled as b). In all numerical experiments discussed below, the latter group represent an ideal monochromatic beam that hits initially the background particles with velocity only in the z-direction $\left(c_z^{(b)}(t=0) = 5\right)$. To get an intuition of the complex non-linear dynamics resulting from the self-consistent computations, we will compare the simulations with a reference experiment, where the Maxwellian distributed BG-particles are not affected by the beam particles. In this sense the distribution function changes only because of the beam particles, which are advanced according to (9), where the non-linear velocity-dependent friction force and diffusion coefficients are obtained exactly by the background characteristics. In fact, this experiment can be considered as an interface between the pure test-particle approach, where the coefficients are held constant for all the particles all the time, and a real simulation. Also in the style of the test-particle approach, we use the mean value

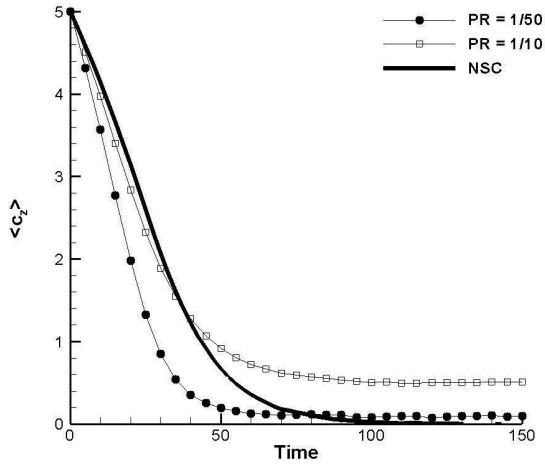

Figure 5. Velocity mean value of the beam particles $< c_z^{(b)}(t) >$ as a function of time for the self-consistent simulations with particle ratios pr=1/50 (line with filled circles) and pr=1/10 (line with open squares) and the non self-consistent reference experiment (full line).

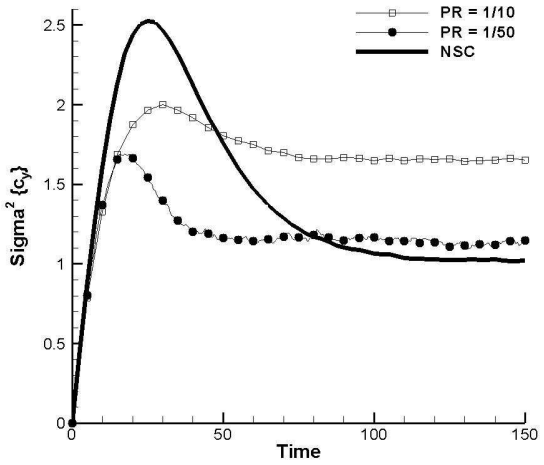

Figure 6. Temporal evolution of the transversal variance $\sigma_y^2(t)$. Full line: reference simulation; line with filled circles: pr=1/50 and line with open squares: pr=1/10 experiment.

$< c_z >$ and the "transversal" variance σ_y^2 of the beam particles as measurable quantities which are recorded as function of time and seen in Figures 5 and 6 as full lines. Moreover, in these Figures the results of two self-consistent simulations ($3 \cdot 10^3$ cycles with $\Delta t = 5 \cdot 10^{-2}$) are depicted, where the beam to background particle ratios (pr) are fixed to pr=1/50 (lines with filled circles) and pr=1/10 (lines with open squares). We remark that in both self-consistent simulations the global velocity distribution functions established by the beam and background particles are highly non-Maxwellian up to $t \leq\sim 35$. In the following we mainly restrict the discussion to the reference experiment and the self-consistent pr= 1/50 simulation.

In order to get better insight of relaxation dynamics we introduce also the beam particle averaged z-component of the friction force

$$\langle F_z(t)\rangle = \frac{1}{N_b}\sum_{i=1}^{N_b} F_z(\vec{c}_i, t) \tag{13}$$

and the "velocity-normalized" yy-component of the diffusion tensor given by

$$\left\langle \frac{D_{22}}{|\vec{c}|}(t)\right\rangle = \frac{1}{N_b}\sum_{i=1}^{N_b} \frac{D_{22}(\vec{c}_i, t)}{|\vec{c}_i(t)|}\ , \tag{14}$$

where N_b is the number of beam particles. Note, that these quantities can be related with the time derivative of the mean value $< c_z >$ and the variance σ_y^2, respectively. The temporal evolution of the friction $\langle F_z(t)\rangle$ and diffusion $\left\langle \frac{D_{22}}{|\vec{c}|}(t)\right\rangle$ coefficients obtained from the reference (full line) and the pr= 1/50 (line with filled circles) simulation are depicted in Figure 7 and 8. By fitting these and the previous curves we tried to extract the time constants τ that characterize the phenomenon and summarized them in the Tables 1 till 4. At first sight we recognize that mean values as well the variances of the three experiments show

$< c_z(t) >$	$\tau_c^{1/50}$	τ_c^{ref}
$t \in [0, 15]$	slow scale dynamics	slow scale dynamics
$t \in [15, 30]$	fast scale dynamics	fast scale dynamics
$t \in [28, 50]$	≈ 12	–
$t \in [30, 90]$	–	≈ 16

Table 1. Time constants τ_c for $< c_z >$

$< F_z(t) >$	$\tau_F^{1/50}$	τ_F^{ref}
$t \in [0, \sim 25]$	transient dynamics	–
$t \in [0, \sim 40]$	–	transient dynamics
$t \in [28, 70]$	≈ 12	–
$t \in [40, 80]$	–	≈ 16

Table 2. Time constants τ_F for $< F_z >$

$\sigma_y^2(t)$	$\tau_\sigma^{1/50}$	τ_σ^{ref}
$t \in [0, 20]$	steep rise up to the max	–
$t \in [0, 30]$	–	steep rise up to the max
$t \in [22, 40]$	≈ 58	–
$t \in [35, 70]$	–	≈ 58

Table 3. Time constants τ_σ for $\sigma_y^2(t)$

$\left\langle \frac{D_{22}}{\vert\vec{c}\vert}(t)\right\rangle$	$\tau_D^{1/50}$	τ_D^{ref}
$t \in [0, \sim 25]$	transient dynamics	–
$t \in [0, 40]$	–	transient dynamics
$t \in [22, 80]$	≈ 10	–
$t \in [40, 120]$	–	≈ 19

Table 4. Time constants τ_D for $\left\langle \frac{D_{22}}{|\vec{c}|}(t)\right\rangle$

approximately the same basic features which appear to be a hint that the underlying relaxation dynamics is essentially similar. However, the relaxation dynamics of the self-consistent experiments are much faster than the reference simulation. This observation seemed to be a direct consequence of the non-Maxwellian global velocity distribution. Note, that the "heating" of the beam particles – which may be considered as a measure of the rapidly increasing asymmetry of the beam particles distribution function (not shown here) – is less pronounced in the self-consistent experiments which seemed to be a consequence of the non-Maxwellian global velocity distribution. The "decay" of these maxima seen in Figure 6 can be associated with further characteristic time scales. It is not surprising that the time constants for the mean value and the variance in perpendicular direction are different. Actually, from the study of the Ornstein-Uhlenbeck

process – the simplest linear diffusion process – it is known that the time constant for the variance is larger than the one for the first moment.[8] Furthermore, we observe that the global velocity distribution of the self-consistent pr= 1/50 simulation is now close to the background Maxwellian of the reference experiment for times $t \geq\sim 35$. Consequently, it seems to be possible that the (fast) initial non-Maxwellian driven relaxation dynamics turn into the Maxwellian dominated equilibrium dynamics. It is obvious from Figure 7, that the

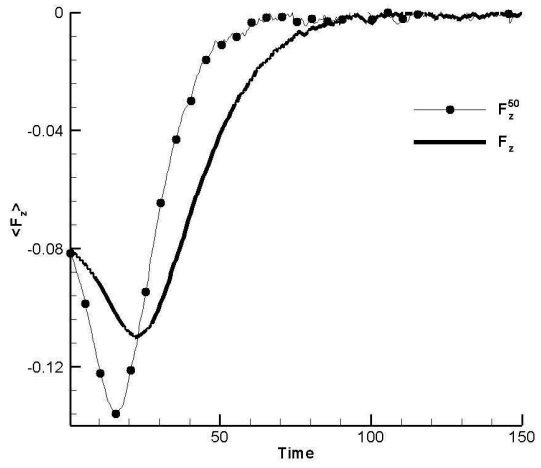

Figure 7. Temporal evolution of the z-component of the averaged frinction force obtained from the reference (full line) and pr=1/50 (line with filled circles) experiment.

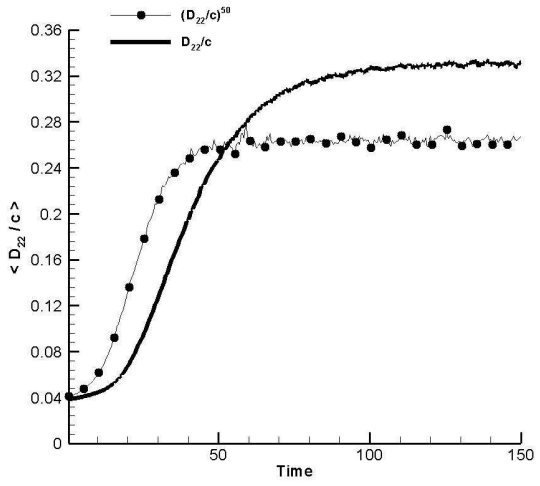

Figure 8. The normalized averaged diffusion coefficient as a function of time computed with the reference (full line) and the self-consistent pr=1/50 (line with filled circles) simulation.

non-Maxwellian global velocity distribution leave its mark especially during the first ~ 30 time units. We recognize there that the shape of the friction coefficient of the pr= 1/50 experiment is different from that one of the refrence simulation and, furthermore, that the self-consistent relaxation dynamics is much faster than in the non self-consistent case. It is interesting that these characteristic initial scales are not seen in the temporal evolution of the diffusion coefficients plotted in Figure 8. On closer inspection of the curves plotted in Figures 7 and 8, we recognize points of inflection located roughly in the intervals $\sim 20 \leq t \leq\sim 30$ and $\sim 30 \leq t \leq\sim 40$ for the pr= 1/50 and non self-consistent simulation, respectively. On the contrary we have found a very good agreement between friction and mean value time constants. At first, it is astonishing that the friction time constant of the self-consistent experiment is also visible in the transversal diffusion coefficient. Under the working hypothesis that the relaxation dynamics turns into a Maxwellian dynamics for $t \geq\sim 35$, we expect a behavior similar to the reference experiment: The onset of the friction and diffusion should start approximately at the same time and the rise of these coefficients should occur at the same characteristic time constant for the pr= 1/50 simulation, that is $\tau_F^{1/50} \approx \tau_D^{1/50}$.

IV. Conclusion and Future Works

In the present paper we have shown that a 3D self-consistent intra-species collisonal relaxation can be effective modeled using the equivalence between the FP equation and a Langevin-type SDE. Friction force and diffusion tensor are evaluated at each time step via 3D Fast Fourier Transform assuring fully self-consistency. A renormalization technique has been adapted for the FP solver in order to drastically reduce the error intrinsically generated by the assignment and interpolation procedure. The presented results of numerical experiments reveal the high quality and reliability of the approximation methods used in the FP solver. Moreover, the dimensionless character of the previous analysis guarantees that it fits perfectly to the study of any kind of charged particles collisions. Inspired by the classical test-particle approach, we

presented a first study of characteristic time constants in self-consistent collisional relaxation. In essence, we identify a fast initially non-Maxwellian driven dynamics which accelerate the relaxation process and seemed to be responsible for short characteristic time constants.

A near future goal concerns the self-consistent simulation of inter-species collisional relaxation. Several powerful approximations are possible which enormously reduce computational costs.
Furthermore, some methodical improvements of the FP solver are desireable. First, we want to explore the various possibilities of reducing the so-called statistical noise, one of the major problems related to particles simulation especially in scarsely populated regions of the velocity space. Remedies in this context are the velocity distribution function averaging over several spatial grid cells or the particle creation and destruction technique. Another cure for noise reduction may be obtained by the fact that the short-time behavior of the distribution function is characterized by a diffusion process. This means, the mean value and variance have to be computed in an appropriate manner to estimate the local velocity distribution function of the particles.
Secondly, a further scientific future goal is the construction of an efficient high order approximation of the multi-dimensional Langevin-type SDE in order to obtain consistent overall accuracy of the FP solver. The starting point to construct high order schemes for SDEs is the stochastic Taylor expansion, which is based on the repeated application of the Itô formula. Such an Itô-Taylor expansion together with the corresponding hierarchical set enables us to retain the correct number of expansion terms for a desired order of the scheme. A certain disadvantage of Itô-Taylor approximations is that the derivatives of various orders of the drift and diffusion coefficients must be determined at each step. To avoid the use of derivatives so-called explicit weak schemes have to be applied.
A main topic in future will be the coupling of the FP solver with fully electromagnetic PIC codes or/and Monte Carlo modules. As mentioned above, an appropriate PIC code for coupling test purposes is already available at IHM. Moreover, a simplified Monte Carlo model based on the P_{null} technique has been already developed and tested at Research Center Karlsruhe. This is thought to be the appropriate basis for the very first coupling tests before the FP module run in parallel with the LasVegas and high order PIC modules coupled together in the PicLas solver to simulate the behavior of the Pulsed Plasma Thruster.

V. Acknowledgments

We gratefully acknowledge the Landesstiftung Baden-Württemberg for funding the present work for two years up to September 2006. Danilo D'Andrea wishes to thank the Forschungszentrum Karlsruhe – in der Helmholtzgemenschaft for the financial support during the year 2007.

References

[1]Auweter-Kurtz, M., Fertig, M., Petkow, D., Stindl, T., Quandt, M., Munz, C.-D., Adamis, P., Resch, M., Roller, S., D'Andrea, D., and Schneider, R., "Development of a hybrid PIC/DSMC Code," IEPC-2005-71, Proceedings of the 29th International Electric Propulsion Conference, Princeton, USA, 2005.

[2]Petkow, D., Fertig, M., Stindl, T., Auweter-Kurtz, M., Quandt, M., Munz, C.-D., Roller, S., D'Andrea, D., and Schneider, R., "Development of a 3-Dimensional, Time Accurate Particle Method for Rarefied Plasma Flows," AIAA-2006-3601, Proceedings of the 9th AIAA/ASME Joint Thermophysics and Heat Transfer Conference, San Francisco, USA, 2006.

[3]Munz, C.-D., Schneider, R., Sonnendrücker, E., Stein, E., Voß, U., and Westermann, T., "A Finite-Volume Particle-In-Cell Method for the Numerical Treatment of the Maxwell-Lorentz Equations on Boundary-Fitted Meshes," *Int. J. Numer. Meth. Engng.*, Vol. 44, 1999, pp. 461–487.

[4]Munz, C.-D., Schneider, R., and Voß, U., "A Finite-Volume Particle-in-Cell Method for the Numerical Simulation of Devices in Pulsed Power Technology," *Surv. Math. Ind.*, Vol. 8, 1999, pp. 243–257.

[5]Laux, M., *Direkte Simulation verdünnter, reagierender Strömungen*, Ph.D. thesis, Institut für Raumfahrtsysteme, Universität Stuttgart, Germany, 1996.

[6]Diver, D., *A Plasma Formulary for Physics, Technology, and Astrophysics*, Wiley-VCH Verlag, Berlin, 2001.

[7]Mitchner, M. and Kruger, C., *Partially Ionized Gases*, Wiley, New York, 1973.

[8]D'Andrea, D., Munz, C.-D., and Schneider, R., "Modeling of Electron-Electron Collisions for Particle-In-Cell Simulations," **FZKA 7218** *Research Report, Forschungszentrum Karlsruhe – in der Helmholtz-Gemeinschaft*, 2006.

[9]Rosenbluth, M., MacDonald, W., and Judd, D., "Fokker-Planck Equation for an inverse-square Force," *Phys. Rev.*,

Vol. 107, 1957, pp. 1–6.

[10]Montgomery, D. and Tidman, D., *Plasma Kinetic Theory*, McGraw-Hill, New York, 1964.

[11]Nicholson, D., *Introduction to Plasma Theory*, Wiley, New York, 1983.

[12]Manheim, W., Lampe, M., and Joyce, G., "Langevin Representation of Coulomb Collision in PIC Simulation," *J. Comput. Phys.*, Vol. 138, 1997, pp. 563–584.

[13]Albright, B., Winske, D., Lemons, D., Daughton, W., and Jones, M., "Quite Simulation of Coulomb Collision," *IEEE Trans. Plasma Sci.*, Vol. 31, 2003, pp. 19–24.

[14]Hassani, S., *Mathematical Physics*, Springer, New York, Berlin, 1999.

[15]Gardiner, C. W., *Handbook of Stochastic Methods*, Springer Verlag, Berlin, Heidelberg, New York, 1985.

[16]Honerkamp, J., *Stochastische Dynamische Systeme*, VCH Verlagsgesellschaft, Weinheim, 1990.

[17]Kloeden, P. and Platen, E., *Numerical Solution of Stochastic Differential Equations*, Springer-Verlag, Berlin, Heidelberg, New York, 1999.

[18]Hockney, R. and Eastwood, J., *Computer Simulation using Particles*, McGraw-Hill, New York, 1981.

[19]Press, W. H., Flannery, B. P., Teukolsky, S. A., and Vetterling, W. T., *Numerical Recipes*, Cambridge University Press, Cambridge, 1987.

[20]Brigham, E., *The Fast Fourier Transform and its Application*, Prentice-Hall, Englewood Cliffs, 1988.

[21]Kloeden, P., Platen, E., and Schurz, H., *Numerical Solution of SDE Through Computer Experiments*, Springer-Verlag, Berlin, Heidelberg, New York, 2003.

[22]Hazeltine, R. and Meiss, J., *Plasma Confinement*, Addison-Wesley, Redwood City, CA, 1991.

[23]Tolman, R., *The Principles of Statistical Mechanics*, Dover Publications, New York, 1979.

[24]Lemons, D., Lackman, J., Jones, M., and Winske, D., "Noise-induced instability in self-consistent Monte Carlo calculations," *Physical Review E*, Vol. 52, 1995, pp. 6855–6861.

[25]Spitzer, L., *Physics of Fully Ionised Gases*, Interscience Publishers, Inc., New York, 1956.

[26]Chandrasekhar, S., *Principles of Stellar Dynamics*, University of Chicago Press, Chicago, 1942.